Journal of Controlled Release 328 (2020) 859–872

Contents lists available at ScienceDirect

Journal of Controlled Release

journal homepage: www.elsevier.com/locate/jconrel

Light-induced release of the cardioprotective peptide angiotensin-(1–9) from thermosensitive liposomes with gold nanoclusters

Julian Bejarano [a,b], Aldo Rojas [a,b,c], Andrea Ramírez-Sagredo [a,c], Ana L. Riveros [a,b], Francisco Morales-Zavala [a,b,c], Yvo Flores [a,b,c], Jaime A. Riquelme [a,b], Fanny Guzman [d], Eyleen Araya [a,e], Mario Chiong [a,c], María Paz Ocaranza [a,f,g], Javier O. Morales [a,f,h], María Gabriela Villamizar Sarmiento [a,h], Gina Sanchez [i], Sergio Lavandero [a,c,i,j,k,*], Marcelo J. Kogan [a,b,j,*]

[a] Advanced Center for Chronic Diseases (ACCDiS), Facultad Ciencias Químicas y Farmaceúticas & Facultad Medicina, Universidad de Chile, Santiago 8380492, Chile
[b] Departamento de Química Farmacológica y Toxicológica, Facultad Ciencias Químicas y Farmacéuticas, Universidad de Chile, Santiago 8380492, Chile
[c] Departamento de Bioquímica, Facultad Ciencias Químicas y Farmacéuticas, Universidad de Chile, Santiago 8380492, Chile
[d] Núcleo de Biotecnología de Curauma (NBC), Pontificia Universidad Católica de Valparaíso, Valparaíso, Chile
[e] Departamento de Ciencias Quimicas, Facultad Ciencias Exactas, Universidad Andres Bello, Santiago 8370035, Chile
[f] Center of New Drugs for Hypertension (CENDHY), Universidad de Chile & Pontificia Universidad Católica de Chile, Santiago 8380492, Chile
[g] División de Enfermedades Cardiovasculares, Facultad Medicina, Pontificia Universidad Católica de Chile, Santiago 8320000, Chile
[h] Department of Sciences and Pharmaceutical Technology, Facultad Ciencias Químicas y Farmaceúticas, Universidad de Chile, Santiago 8380492, Chile
[i] Instituto de Ciencias Biomédicas (ICBM), Facultad Medicina, Universidad de Chile, Santiago 8380453, Chile
[j] Corporación Centro de Estudios Científicos de las Enfermedades Crónicas (CECEC), Santiago 7680201, Chile
[k] Department of Internal Medicine (Cardiology Division), University of Texas Southwestern Medical Center, Dallas, TX 75390–8573, USA

ARTICLE INFO

Keywords:
Angiotensin-(1-9)
Cardioprotection
Cardiovascular diseases
Thermosensitive liposomes
Nanoparticles

ABSTRACT

Angiotensin-(1-9), a component of the non-canonical renin-angiotensin system, has a short half-life in blood. This peptide has shown to prevent and/or attenuate hypertension and cardiovascular remodeling. A controlled release of angiotensin-(1-9) is needed for its delivery to the heart. Our aim was to develop a drug delivery system for angiotensin-(1-9). Thermosensitive liposomes (LipoTherm) were prepared with gold nanoclusters (LipoTherm-AuNC) to increase the stability and reach a temporal and spatial control of angiotensin-(1-9) release. Encapsulation efficiencies of nearly 50% were achieved in LipoTherm, reaching a total angiotensin-(1-9) loading of around 180 μM. This angiotensin-(1–9)-loaded LipoTherm sized around 100 nm and exhibited a phase transition temperature of 43 °C. AuNC were grown on LipoTherm and the new hybrid nanosystem showed energy absorption in the near-infrared (NIR) wavelength range. By NIR laser irradiation, a controlled release of angiotensin-(1-9) was achieved from the LipoTherm-AuNC nanosystem. These nanosystems did not show any cytotoxic effect on cultured cardiomyocytes. Biological activity of angiotensin-(1-9) released from the LipoTherm-AuNC-based nanosystem was confirmed using an *ex vivo* Langendorff heart model.

1. Introduction

Cardiovascular diseases (CVD) are currently the leading cause of death globally [1]. Both coronary artery disease (CAD) and hypertension (HT) are the most common causes of CVD [2,3]. Moreover, CAD is the main cause of myocardial infarction (MI) [3]. Heart and blood vessels are affected through pathological structural and functional remodeling, resulting in heart failure (HF) [4]. Pathological cardiovascular remodeling is a process where arteries and heart suffer irreversible structural and functional changes regularly associated with overactivation of the renin-angiotensin system (RAS), and the adrenergic system [5]. Deregulation of the RAS system by angiotensin II (Ang II) or aldosterone significantly contributes to the pathophysiology of CVD and perpetuates cascades of pro-inflammatory, pro-hypertrophic, atherogenic and pro-

* Corresponding authors at: Advanced Center for Chronic Diseases (ACCDiS), Facultad Ciencias Químicas y Farmaceúticas & Facultad Medicina, Universidad de Chile, Santiago 8380492, Chile.
E-mail addresses: slavander@uchile.cl (S. Lavandero), mkogan@ciq.uchile.cl (M.J. Kogan).

https://doi.org/10.1016/j.jconrel.2020.11.002
Received 18 May 2020; Received in revised form 11 October 2020; Accepted 1 November 2020
Available online 4 November 2020

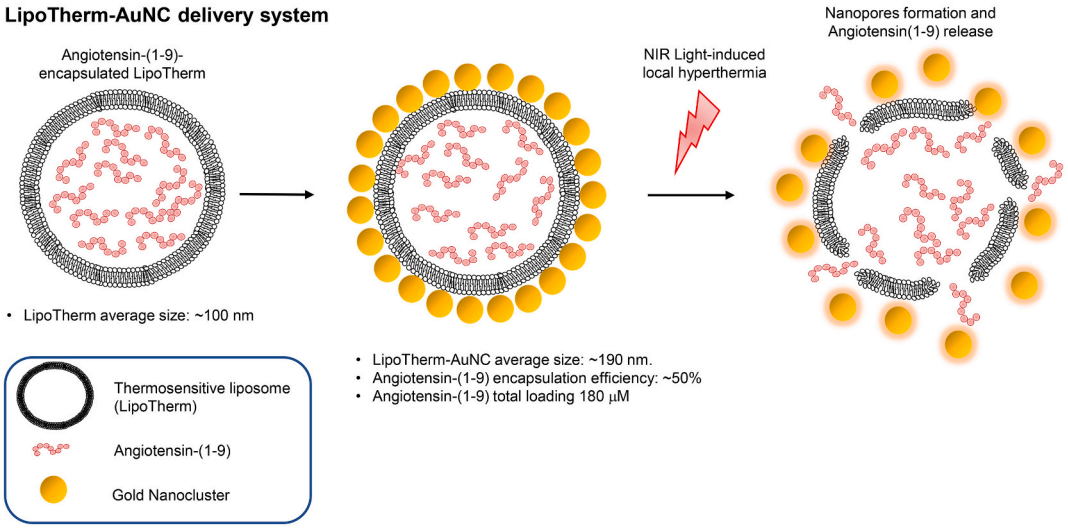

Fig. 1. Schematic diagram of Ang-(1-9) encapsulation and its NIR light-induced controlled release from gold-coated thermosensitive liposomes. (For interpretation of the references to color in this figure legend, the reader is referred to the web version of this article.)

thrombotic effects triggering end-organ damage [6,7]. In recent decades, the efficacy of the therapeutic agents targeted to the RAS has greatly improved cardiovascular clinical outcomes by suppressing cardiac hypertrophy, fibrosis and improving electromechanical function [8]. The 9-aminoacid peptide angiotensin-(1-9) [Ang-(1-9)] is a component of the counter-regulatory axis of the RAS [9]. We and others have shown that Ang-(1-9) exerts cardiovascular protective effects, by decreasing myocardial damage induced by ischemia/reperfusion, adverse cardiovascular remodeling and inflammation triggered by HT [10–17]. However, these beneficial actions of Ang-(1-9) are limited by its short half-life in circulation caused by enzymatic degradation. In our *in vivo* studies, we have used osmotic mini-pumps for a sustained infusion-like administration of Ang-(1-9) to show its beneficial effects [11,12]. Accordingly, alternative strategies that enable less invasive and controlled drug delivery are required for its clinical translation.

Nanomedicine provides unique approaches to pack, protect and transport drugs and biomolecules, as well as control their delivery to specific sites with high versatility and potential to reduce systemic toxicity and increase therapeutic efficacy [18]. The evidence has shown that nanocarrier drug formulations are useful to provide controlled delivery of therapeutic agents in cardiovascular applications [19–22]. For example, the "enhanced permeability and retention" (EPR) effect, achieved by the use of nanoparticles, enhances the passive accumulation in inflammation regions. Ichimura et al. showed in a porcine model that the EPR effect is useful for the accumulation of pitavastatin-loaded PLGA nanoparticles in the infarcted myocardial region and this nanosystem was further able to deliver the drug efficiently [23].

Liposomes are extensively considered as appropriate nanocarriers for cardiovascular drug delivery because of their physicochemical versatility, biodegradability, biocompatibility (non-toxic, non-hemolytic and non-immunogenic) and their recognized potential for targeted and controlled release [21,24–27]. Liposomes can carry their load into their lipid bilayer or aqueous core, while protecting its degradation in the body [24–27]. In other studies, certain cardioprotective peptides, including angiotensin- [1–7] and [Pyr1]-apelin-13, have been encapsulated into liposomal formulations to increase their stability and protect them from enzymatic degradation in the blood [24,28,29].

By using liposomes to encapsulate therapeutic agents, higher stability and long-circulating properties can be achieved. The so-called EPR effect, due to particle size and avoidance of the clearing mechanisms for exogenous particle elimination, enables nanocarriers for long circulating times, extravasation in leaky sites in the body (associated with inflammation [30] and tumors [31]), and accumulation in such sites, leading to improved accumulation at damaged sites [32]. However, the encapsulated therapeutic agent can lose bioavailability due to its low release efficiency from liposomes, or slow passive diffusion through the lipid bilayer [33]. In turn, it is often challenging to combine high drug stability in the bloodstream with a rapid and optimal spatiotemporal release at the target site [34]. In the case of Ang-(1-9), this peptide should have an efficient and controlled spatio-temporal release from the liposome as its therapeutic effect highly depends on extracellular availability and direct binding to the AT_2 extracellular membrane receptor [13].

Thermosensitive liposomes are a useful alternative to increase drug release efficiency when used along with local mild hyperthermia of a few degrees above the average normal body temperature (40–43 °C), but enough to modify the liposome bilayer properties to enable drug release [35]. This conformational change in the lipid bilayer structure is produced in response to a higher energy state during the gel-to-liquid phase transition at the transition temperature (T_m), which leads to an increased volume in the lipid bilayer and a subsequent increase of its permeability [36]. Moreover, with the incorporation of lysolipids like MSPC (1-stearoyl−2-hydroxy-sn-glycerol-3-phosphocholine) into the lipid bilayer structure of liposomes, it has been possible to increase the loaded amount and speed up the release of the therapeutic agent from the aqueous core by the formation of nanopores inside the lipid bilayer at the T_m [36]. However, it is often difficult to achieve an adequate local temperature control in a clinical setting [37]. Therefore, in order to obtain a controlled hyperthermia for spatial and temporal control release, plasmonic nanoparticles, such as gold nanostructures deposited onto the surface of the liposome can be used for producing a mild local hyperthermia around the liposomes after near-infrared (NIR) irradiation, which induces the phase transition in the lipid bilayer at T_m, increasing its permeability and leading to an increased and faster release of the cargo [38–40]. Light-controlled release using a catheter or endoscopic light may allow precise, on-demand content delivery in a precise intervention *in vivo* [37].

Liposomes coated with gold nanoclusters (AuNC) have gained attention because of their optical absorption in NIR, which allows a non-invasive therapy with greater light penetration into human tissues during irradiation, without causing damage (the so-called "biologically friendly" NIR window) [40,41] (Fig. 1). Moreover, the degradation of these gold-liposome hybrid nanosystems allows the disaggregation of the gold clusters toward gold nanoparticles of about 6 nm, which meet the requirements for renal excretion [38]. Therefore, NIR light-induced release from gold-liposomes nanosystems would offer spatial and

temporal control for the Ang-(1-9) delivery.

The present study was aimed to develop thermosensitive liposomes (LipoTherm) coated with AuNC to encapsulate Ang-(1-9) and evaluate its release induced by NIR light. We also evaluated the cytocompatibility and biological activity of Ang-(1-9) released from the nanosystem using an *ex vivo* Langendorff heart rat model. To our knowledge, the light-controlled release of cardioprotective peptides using a nanosystem based on thermosensitive liposomes with gold nanoparticles has not been described yet. Thus, this study shows relevant insights about the design of novel nanosystem formulations for controlled drug delivery in the field of CVD.

2. Materials and methods

2.1. Reagents

Ang-(1-9) was synthetized using a solid-phase method and provided by Acuapeptide Synthesis (Núcleo de Biotecnología de Curauma, Pontificia Universidad Católica de Valparaíso, Valparaíso, Chile). 1,2-Dipalmitoyl-sn-glycero-3-phosphatidylcholine (DPPC), 1,2-distearoyl-sn-glycero-3-phosphatidylcholine (DSPC), 1-myristoyl-2-stearoyl-*sn*-glycero-3-phosphocholine (MSPC or lyso-SPC) and 1,2–distearoyl-sn-glycero-3-phosphatiylethanol-amine-N-[methoxy (polyethylene glycol)-2000] (DSPE-PEG2000) were purchased from Avanti Polar Lipids (Alabaster, AL). Chloroform, Triton X-100 and D-glucose monohydrate were obtained from Merck (Darmstadt, Germany). Hydrogen tetrachloroaureate (III) hydrate ($HAuCl_4$*xH_2O, 99.995%) and L-ascorbic acid (BioXtra, ≥ 99.0%) were purchased from Sigma-Aldrich (St. Louis, MO). Nitrogen gas was provided by Linde S.A, Chile. All chemicals and solvents were of analytical grade and used without further purification. Milli-Q water (Millipore Corp, MA) was used for all aqueous solutions. All glassware used for gold reduction was washed with aqua regia and extensively rinsed with Milli-Q water.

2.2. Synthesis and characterization of the Ang-(1-9) peptide

Peptide sequence was synthesized using the Fmoc/tBu strategy. A wang resin (loading 0.6 mmol/g) was used as the solid support and the attachment of the first amino acid was performed by using diisopropyl carbodiimide and 4-dimethylamino pyridine(DIC/DMAP) to avoid racemization. [42]. One synthesis cycle was composed of Fmoc-deprotection and coupling. Standard couplings of amino acids were carried out in dimethylformamide (DMF) solvent using a mix of an activating agent (2-(1H-benzotriazol-1-yl)-1,1,3,3-tetramethyluronium hexafluorophosphate (HBTU)/ OxymaPure®), Fmoc-protected amino acid and the tertiary base diisopropilethylamine (DIPEA), in proportions of 3:3:4.5 equivalents, respectively (one synthesis cycle was 3 h). For the amino acid arginine, double couplings were made; the second coupling was with *N*,*N*,*N*′,*N*′-Tetramethyl-O-(benzotriazol-1-yl)uronium tetrafluoroborate (TBTU)/ Oxymapure /DIPEA. The deprotection was performed with 20% piperidine in DMF (2 × 7 min).

After completing synthesis, the peptide was cleaved from the solid support using trifluoroacetic acid (TFA), under gentle agitation over a period of 3 h at room temperature, in the presence of scavengers (standard cleavage solution: TFA/Triisopropylsilane (TIS)/water 95:2.5:2.5). After filtration the crude peptides were precipitated by the addition of cold diethyl ether (Et_2O), centrifuged, washed with cold Et_2O five times, dried, dissolved in ultrapure water, frozen, and lyophilized. The C-terminal end of the peptide was obtained as free carboxylic acid. The peptide was purified using a C18 column. Characterization of the Ang-(1-9) peptide was made by high performance liquid chromatography (HPLC) to verify purity and ESI-MS mass spectrometry to confirm identity, using a LCMS-2020 ESI-MS (Shimadzu Corp., Kyoto, Japan), with a column XBridge BEH130 C18 3.5 μm dp, 4.6 × 100 mm and a gradient of 0–70% acetonitrile-water in 8 min. Supplementary Fig. 1 shows the corresponding spectra.

2.3. Preparation of Ang-(1–9)-loaded thermosensitive liposomes (LipoTherm)

Thermosensitive liposomes, called LipoTherm, were prepared using the thin-lipid film hydration method followed by extrusion, with a lipid composition able to exhibit temperature-sensitive controlled release similar to one previously described [43]. DSPC was added to obtain liposomes with a phase transition temperature (T_m = 43 °C) slightly higher than that reported using DPPC (T_m = 42 °C) in order to avoid drug leakage produced by phase transition onset near body temperature. Therefore, the membrane was composed of DPPC, DSPC, MSPC and DSPE-PEG_{2000} in a 71:15:10:4 M ratio. Briefly, the proper amounts of dry lipids were solubilized in chloroform and dried with nitrogen gas and temperature to ensure solvent removal. The resulting dry lipid film was then hydrated (24 mM lipid concentration) with a 0.3 M hyperosmotic aqueous glucose solution containing 200, 300 or 400 μM of Ang-(1-9) at 53 °C (nearly 10 °C above the gel-to-liquid phase transition temperature), alternating with vortex agitation for 30 min. After hydration, the liposomal suspension was subjected to sequential extrusion (mini-extruder, Avanti, AL) at the same hydration temperature through polycarbonate membranes (Nucleopore, Whatman, NJ) of decreasing pore size (400, 200 and 100 nm). Twenty extrusion cycles were performed for each pore size to obtain homogeneous unilamellar vesicles. The liposomal suspension was then dialyzed by adding 2 mL into a dialysis cellulose bag (molecular weight cut off [MWCO] 10 kDa, Sigma-Aldrich, USA). The dialysis bag was clamped and suspended in 1 L PBS, pH 7.4 (release medium), at room temperature and rotated at 150 rpm. The dialysis system was kept overnight and on the following day, the dialysis medium was changed twice every 3 h. A second step of purification by diafiltration was required for a more effective removal of the non-encapsulated Ang-(1-9). Preliminary data of this study showed that after purifying only by dialysis, an amount of up to 10 μM of non-encapsulated Ang-(1-9) remained, while by adding the diafiltration step, no residual Ang-(1-9) was detected (its presence can hinder the gold reduction process). The diafiltration system (Amicon, EMD Millipore Corporation, MA, USA) consisted of a diafiltration cell (10 mL capacity, Amicon 8010) with a magnetic stirrer (100 rpm), a regenerated cellulose membrane (MWCO 5 kDa, 25 mm diameter), a reservoir (1 L capacity), a selector, and a pressure source (3 bar). The purification was performed for 3 h by passing a continuous flux of PBS from the reservoir through the diafiltration cell, which contained 2 mL of liposomal suspension. Finally, the resulting liposomal formulations were stored at 4 °C until characterization or the subsequent gold reduction stage.

2.4. Physicochemical characterization of Ang-(1–9)-loaded LipoTherm

Particle size distribution and surface charge of the Ang-(1–9)-loaded liposomes were evaluated by dynamic light scattering (DLS) using a Zetasizer Nano ZS system (Malvern Instruments, UK). Liposome concentration was determined by nanoparticle tracking analysis (NTA) using a NanoSight NS300 instrument (NanoSight, Amesbury, UK). Liposome T_m was analyzed by differential scanning calorimetry (DSC) using a Perkin Elmer DSC 6000 microcalorimeter with sealed pans, operating at a scan rate of 5 °C/min for both heating and cooling cycles (two cycles each), spanning the temperature range of 4–80 °C. Transmission electron microscopy (TEM) images were obtained in a transmission-mode scanning electron microscope (TSEM, FEI Inspect 50). A drop of the liposomal dispersion was placed on formvar/carbon-coated copper grids and then stained with 0.5% phosphotungstic acid, before TSEM evaluations.

2.5. Evaluation of the encapsulation efficiency of Ang-(1-9)

In order to evaluate the encapsulation efficiency and total Ang-(1-9) encapsulated inside the liposomes, the liposomal formulations were previously treated with a solution of 0.5% Triton® X-100 at 50 °C for 1 h

to disrupt the lipid bilayer and release the encapsulated Ang-(1-9). Ang-(1-9) concentration was measured by high-performance liquid chromatography (HPLC) using a Flexar™ Perkin Elmer instrument with a C18 analytical column XBridge™ peptide BEH130 (130 Å, 3.5 μm, 4.6 × 100 mm, Waters, USA), at 25 °C. The mobile phases consisted of acetonitrile (A) and 0.045% trifluoroacetic acid in deionized water (B). We employed a detection wavelength of 220 nm and a flow rate of 0.9 mL/min, with gradient elutions from 5% of A and 95% of B to 100% of B, over 20 min. Under these conditions, Ang-(1-9) had an elution time of 11 min and its concentration was calculated from the peak area using an equation obtained through a standard curve.

2.6. Evaluation of free and encapsulated Ang-(1-9) stability

Stability of free and encapsulated Ang-(1-9) was evaluated with a test performed in heat-inactivated fetal bovine serum (FBS). A 120 μM free Ang-(1-9) solution and a sample of liposomes (24 mM lipid concentration) loaded with the same Ang-(1-9) concentration were diluted five times in FBS, maintained at 37 °C and centrifuged at 300 rpm for 5, 10, 30, 60 and 120 min. After each time point, an aliquot was taken and dissolved two times in a methanol/5% Triton X-100 (4:1 ratio) solution and left at least 20 min at 4 °C with subsequent centrifugation at 13,000 *g* for 30 min to precipitate proteins. The supernatant was maintained at 50 °C for 30 min to allow complete extraction of Ang-(1-9) from the liposomes and Ang-(1-9) concentration was quantified by HPLC, as described above.

2.7. Temperature-induced release of Ang 1–9 from LipoTherm

The *in vitro* release of entrapped Ang-(1-9) from LipoTherm at T_m was determined at 5, 10, 20, 40 and 80 min. We then evaluated the effect of the initial Ang-(1-9) concentration (200, 300 and 400 μM) on the maximum Ang-(1-9) loading, encapsulation efficiency and release profile. Briefly, 200 μL of liposomal suspension in PBS were placed into separate tubes for each time point, and incubated in a water bath at 43 °C for the designated time period. After each heating period, the samples were quenched in cold water (2 min), then diluted twice with PBS, and centrifuged for 1 h at 226,800 g to obtain a liposomal pellet. Supernatants were then analyzed by HPLC to measure the concentration of Ang-(1-9) released at each time period ($n = 3$).

2.8. Reduction of gold on the Ang-(1–9)-loaded LipoTherm: development of LipoTherm-AuNC

The reduction of a gold salt and subsequent formation of gold nanoclusters (AuNC) onto the liposome surface was achieved using a similar process previously reported [38,39,44]. Briefly, aqueous solutions of 100 mM auric chloride and 500 mM ascorbic acid were obtained. To get resonance wavelengths in the NIR of around 750 nm, 12 μL of auric chloride 100 mM and 18 μL of ascorbic acid 500 mM were added to 1 mL of the previously prepared Ang-(1–9)-loaded liposome formulations in PBS (24 mM lipid concentration and 140 μM Ang-(1-9). First, the gold solution was added and gently swirled for 2 min until a homogeneous solution is achieved. Then, ascorbic acid was added and gently magnetic stirred until a blue color appeared. Finally, the resulting blue dispersions were left stirring for 6 min. Following the gold reduction step, the gold-coated liposomes (LipoTherm-AuNC) were dialyzed twice against PBS to remove any residue of the starting solutions. Briefly, 1 mL of LipoTherm-AuNC was added into a dialysis cellulose bag (10 kDa MWCO, Sigma-Aldrich, USA). The dialysis bag was suspended in 1 L PBS, pH 7.4 (release medium), at room temperature and rotated at 150 rpm. The dialysis system was kept overnight and on the following day, the dialysis medium was changed twice every 3 h.

2.9. Physico-chemical characterization of the Ang-(1–9)-loaded LipoTherm-AuNC nanosystems

Gold-coated liposomes were characterized by NTA, DLS and TEM to evaluate their size distribution, nanoparticle concentration, surface charge and morphology. TEM images were obtained with a HT7700 model microscope (Hitachi) operated at 100 kV and a high resolution microscope (HR-TEM) FEI Tecnai G^2-F20, operated at 200 kV and equipped with X-ray energy dispersive spectroscopy (XEDS) to confirm the presence of the gold nanoparticles and their interaction with the liposomes. UV − vis spectroscopy using a Lamba 25 instrument (Perkin Elmer, MA) was used to evaluate the absorption spectra of the gold nanoclusters grown on LipoTherm. The degradation of the gold-coated LipoTherm was evaluated by DLS and TEM after lysis of the lipid bilayer with 1% Triton X-100 at 50 °C for 1 h.

2.10. Light-induced release of Ang-(1-9) from the LipoTherm-AuNC nanosystems

The light-induced release of Ang-(1-9) from the previously prepared LipoTherm-AuNC nanosystems (24 mM lipid concentration and 140 μM Ang-(1-9)) was conducted in a custom -made temperature- controlled chamber at 37 °C. Briefly, 200 μL of Ang-(1–9)-loaded LipoTherm-AuNC was placed into a glass tube and maintained under magnetic stirring to guarantee homogeneity during laser illumination. The illumination was obtained from an 808 nm continuous wave NIR laser source, at 350 mW (Power Technology Inc., AR) and the sample was irradiated from the top, so as to directly interact with the sample for 2.5, 5, 10, 20 and 40 min. A thermal imaging infrared camera series LT3 (Zhejiang DALI Technology Co. Ltda, China) was used to record the local temperature changes in the samples during laser illumination. After each irradiation period, the sample was quickly quenched in cold water for 2 min to stabilize the liposomes and prevent further release of Ang-(1-9). The samples were then centrifuged for 1 h at 226,800 g to get a LipoTherm-AuNC pellet. Supernatants were then analyzed by HPLC to quantify Ang-(1-9) release during each irradiation time period ($n = 3$).

2.11. Preparation and culture of neonatal rat ventricular myocytes (NRVM)

All experiments were performed in agreement with the Guide for the Care and Use of laboratory Animals published by the US National Institutes of Health (2016) and were approved by the Institutional Ethics Review Committees from Universidad de Chile (CBE2015-29 and 18,164-CYQ-UCH). Adult male and 1–3 day-old Sprague Dawley rats were obtained from the Animal Breeding Facility of the Faculty of Chemical and Pharmaceutical Sciences, Universidad de Chile. NRVM were isolated as described in [45]. Cells were pre-plated for 2 h in plastic Petri dishes to discard non-myocyte cells. The cardiomyocyte-enriched fraction was plated on gelatin-precoated 35 mm plates and grown in DMEM/M199 (4:1) medium containing 10% (*w/v*) fetal bovine serum (FBS) and bromodeoxyuridine (100 mM) for 24 h before the experiments.

2.12. Evaluation of cytotoxicity

The cytotoxic effect of the Ang-(1–9)-loaded LipoTherm-AuNC nanosystems was evaluated by measuring the activity of lactate dehydrogenase (LDH) by spectrophotometry at 490 nm in samples of the culture medium after 24 h of incubation with the different stimuli, using the CytoTox 96® Non-Radioactive Cytotoxicity Assay kit, (Promega Corp., Madison, WI), according to the manufacturer's instructions. To evaluate cell death, NRVM were randomly assigned to the following conditions: a) control: MM with 10% (*w/v*) fetal bovine serum (FBS); b) positive control using hydrogen peroxide 2%; c) empty LipoTherm; d) free Ang-(1-9) (1 μM); e) empty LipoTherm-AuNC system; f) Ang-(1–9)-

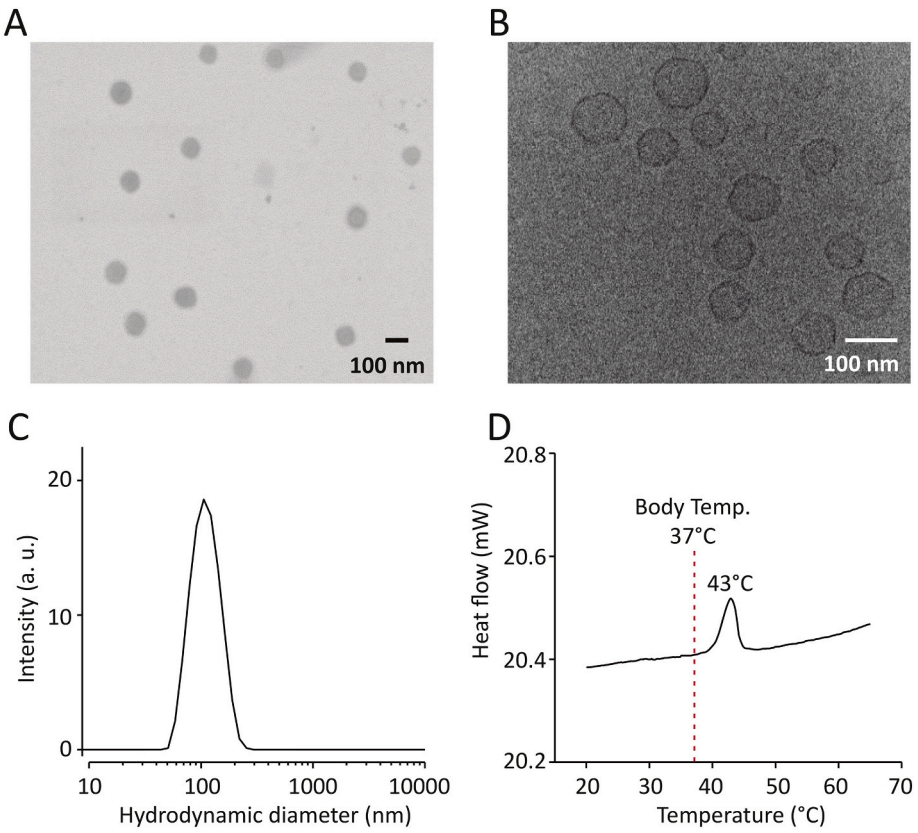

Fig. 2. Characterization of Ang-(1–9)-loaded LipoTherm by: (A) Scanning transmission electron microscopy (STEM), (B) Cryo-transmission electron microscopy (TEM), (C) Dynamic light scattering (DLS) and (D) Differential scanning calorimetry (DSC).

loaded LipoTherm-AuNC; g) Ang-(1–9)-loaded LipoTherm-AuNC system with laser irradiation (808 nm, 350 mW) for 10 min and h) irradiated control (MM with 10% (w/v) FBS.

2.13. Ex vivo evaluation of Ang-(1-9) released from the LipoTherm-AuNC nanosystem

Non-toxic and cardiac functional effects of Ang-(1–9)-loaded LipoTherm-AuNC were investigated in isolated hearts from adult male Sprague-Dawley rats (250 g) subjected to a perfusion protocol using the Langendorff retrograde perfusion method [46]. Rats were anesthetized with pentobarbital [80 mg/kg i.p.] and heparin 100 U/kg was injected into the right atria. Hearts were perfused retrogradely through the aorta with Krebs-Henseleit (KH) buffer containing: 128.3 mM NaCl, 4.7 mM KCl, 1.35 mM $CaCl_2$, 1.1 mM $MgSO_4$, 20.2 mM $NaHCO_3$, 0.4 mM NaH_2PO_4 and 11.1 mM glucose, pH 7.4 (equilibrated with a 95% O_2/5% CO_2 at 37 °C), using a peristaltic pump (Gilson Miniplus 3, France). A latex balloon (filled with saline solution) connected to a pressure transducer was placed through the left atrium and mitral valve into the left ventricle in order to assess isovolumetric intraventricular pressure. Perfusion flow was 10–14 mL/min and hearts were paced at 240–300 beats/min with platinum electrodes, using a temperature-controlled chamber and a Grass stimulator (pulses of 5 V, 1 ms). The following cardiac parameters were continuously monitored: left ventricular (LV) developed pressure (LVDP), LV end-diastolic pressure (LVEDP; set at 5–10 mmHg at the beginning of the experiment). A volume of 200 μL of both empty nanosystem and with Ang-(1-9) (10 μM) was laser irradiated (808 nm, 350 mW) for 10 min and dissolved 2.5 times in PBS buffer, with subsequent centrifugation at 226,800 *g* for 1 h at 4 °C. The supernatant was analyzed by HPLC, as described above. The hearts were perfused with a solution of the released Ang-(1-9) (50 μL of released Ang-(1-9) (1.6 μM) was dissolved in 150 mL of KH buffer a final concentration 0.5 nM). Adult rat hearts were randomly assigned to the following groups: a) Control: hearts were perfused with the KH buffer for 20 min; b) Ang-(1-9): hearts were stabilized for 20 min, followed by perfusion with 50 nM Ang-(1-9); c) Lipo-Au: Hearts were stabilized for 20 min, followed by perfusion with supernatant post irradiation from empty LipoTherm-AuNC nanosystem; d) Lipo-Au-Ang 1–9: Hearts were stabilized for 20 min, followed by perfusion with supernatant 0,5 nM Ang-(1-9) post irradiation from loaded LipoTherm-AuNC. Cardiac parameters were continuously monitored with pressure transducers: LVDP, LVEDP and maximum rate of LV pressure increase (+dP/dt).

2.14. Statistical analysis

Data are presented as the mean ± standard deviation (SD), and the resulting values from each experiment were subjected to 2-way Kruskal-Wallis test and Dunn's Multiple Comparison post-analysis. Differences with values of $p<0.05$ were considered as statistically significant.

3. Results and discussion

3.1. Ang-(1–9)-loaded thermosensitive liposomes

Ang-(1-9) was efficiently loaded into an optimized thermosensitive liposomal composition using the thin-lipid film hydration method followed by extrusion, which allows payloads up to 183 μM of Ang-(1-9), encapsulation efficiency (EE) of about 50% and monodisperse size distributions, with average particles size around 100 nm. Additionally, the purification processes with ultrafiltration and dialysis allowed to obtain an appropriate liposomal dispersion for the subsequent gold reduction step, which would be highly affected by the presence of a significant residual amount of non-encapsulated Ang-(1-9). Fig. 2 shows the characterization of the Ang-(1-9) loaded LipoTherm. The liposomal

Table 1
Summary of the Ang-(1–9)-loaded LipoTherm properties.

Property	
Average size (nm)	107 ± 38
Polydispersity index	0.08
Concentration (liposomes/mL)	$6.4 \times 10^{12} \pm 1.9 \times 10^{7}$
Z potential (mV)	-2 ± 3
Phase transition temperature (°C)	43

Table 2
Effect of the Ang-(1-9) dosed during the LipoTherm preparation on total loading and encapsulation efficiency.

Dosed Ang-(1-9) (μM)	Total loaded Ang-(1-9) (μM)	Encapsulation efficiency (%)
200	107	54
300	153	51
400	183	46

dispersion was composed by nanovesicles around 100 nm of diameter, as shown in the TSEM image (Fig. 2A). Cryo-TEM confirmed the average particle size shown by TEM and the unilamellar structure and lipid bilayer of the liposomes was further observed in detail (Fig. 2B). The information about the liposome particle size obtained by TEM was further supported by DLS analysis (Fig. 2C), which showed a monodisperse size distribution, with an average hydrodynamic particle size of 107 nm (Table 1). Additionally, the liposome concentration evaluated by NTA was 6.4×10^{12} liposomes/mL for a lipid concentration of 20 mg/mL. Ang-(1–9)-loaded LipoTherm exhibited a surface charge of −2 mV (Table 1) in PBS (pH = 7.4), which is consistent with the neutral lipids of the liposome composition (DPPC, DSPC, MSPC and DSPE-PEG). A summary of the liposome properties is shown in Table 1.

Liposomal dispersion showed high colloidal stability in PBS at 4 °C for at least one month, maintaining its nanometric particle size, neutral surface charge and steric stabilization by the PEG (Supplementary Table S1).

The phase transition temperature (T_m) is an important property in thermosensitive liposomes because it determines the onset of the liquid disordered phase state in the lipid bilayer, which is characterized by an increased permeability of the entrapped compounds [36]. The permeability is greatest around T_m due to the coexistence of membrane areas in both solid gel and liquid disordered phases [47]. DSC was used to identify the T_m of the LipoTherm sample (Fig. 2D), showing an approximate T_m at 43 °C, with onset and endset temperatures of 40 and 45 °C, respectively. The onset of the phase transition at 40 °C, *i.e.* above body temperature (37 °C), helps to avoid Ang-(1-9) leakage *in vivo* because at 37 °C the lipid bilayer of the liposomes is in a solid gel phase (L_β) of low permeability [48].

The encapsulation of Ang-(1-9) inside the LipoTherm was performed using three different concentrations of this peptide (200, 300 and 400 μM) to evaluate their effect on the total loading (TL) and EE. Table 2 shows the values of TL and EE for each dosed Ang-(1-9) concentration. EE was about 50%, showing a slight decrease when the dosed concentration increased. On the other hand, the TL was above 100 μM, reaching concentrations around 180 μM for the maximum dosed concentration (400 μM). This evaluation allowed to find the initial Ang-(1-9) concentration necessary for the desired liposome loading in subsequent cell tests or therapeutic evaluations. The absence of a concentration-dependent response upon increasing amounts of Ang-(1-9) could be associated with working conditions close to the drug saturation content of the system [49].

3.2. Stability of free and LipoTherm-encapsulated Ang-(1-9)

One of the main goals of encapsulating the Ang-(1-9) peptide inside the LipoTherm was to protect it from metabolic degradation in the blood after systemic administration. Serum proteases usually cleave peptide bonds in seconds or minutes, so these peptides have high clearance and poor pharmacokinetics. Ang-(1-9) is a specific substrate for angiotensin converting enzyme (ACE), producing Ang-1-7 [50]. The stability of Ang-(1-9), either in free or encapsulated form, was evaluated by exposure to FBS and the residual or non-degraded Ang-(1-9) concentration was measured by HPLC after 5, 10, 30, 60 and 120 min (Fig. 3). Residual Ang-(1-9) was calculated as a percentage respect to the total Ang-(1-9) concentration present at the beginning of the test.

The results in Fig. 3 show that after 10 min in FBS, both free and encapsulated Ang-(1-9) suffered degradation to some extent, remaining 82% and 75% of the initial Ang-(1-9) concentration for the encapsulated and free Ang-(1-9), respectively. This could be associated with Ang-(1-9) availability in the external surface of the lipid bilayer, enabling its degradation when exposed to FBS. As time increased, free Ang-(1-9) suffered a greater degree of degradation since the residual amount decreased to 27% at 60 min, and completely decreased after 120 min in FBS. Conversely, Ang-(1-9) encapsulated inside LipoTherm was protected from degradation in FBS and the residual concentration inside liposomes was maintained above 80% until 120 min. These results confirm that the stability of Ang-(1-9) in serum can be increased by its

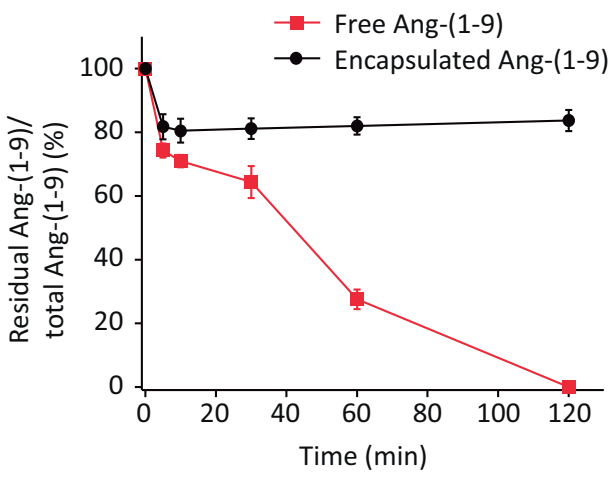

Fig. 3. Stability of free and LipoTherm-encapsulated Ang-(1-9).

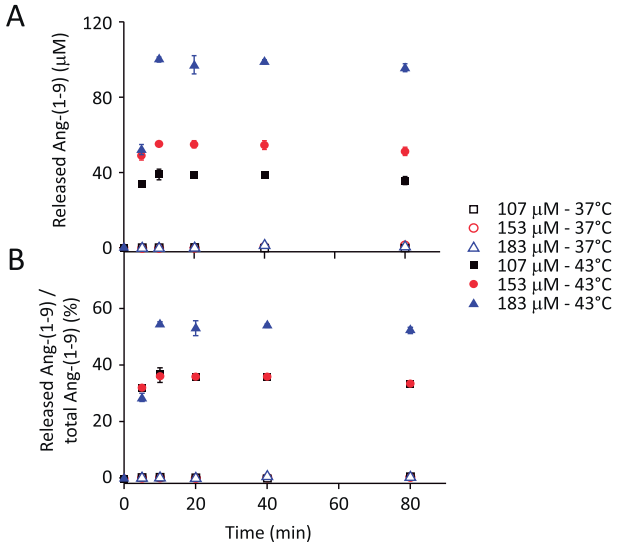

Fig. 4. Effect of temperature and Ang-(1-9) concentration on the release of Ang-(1-9) over time.

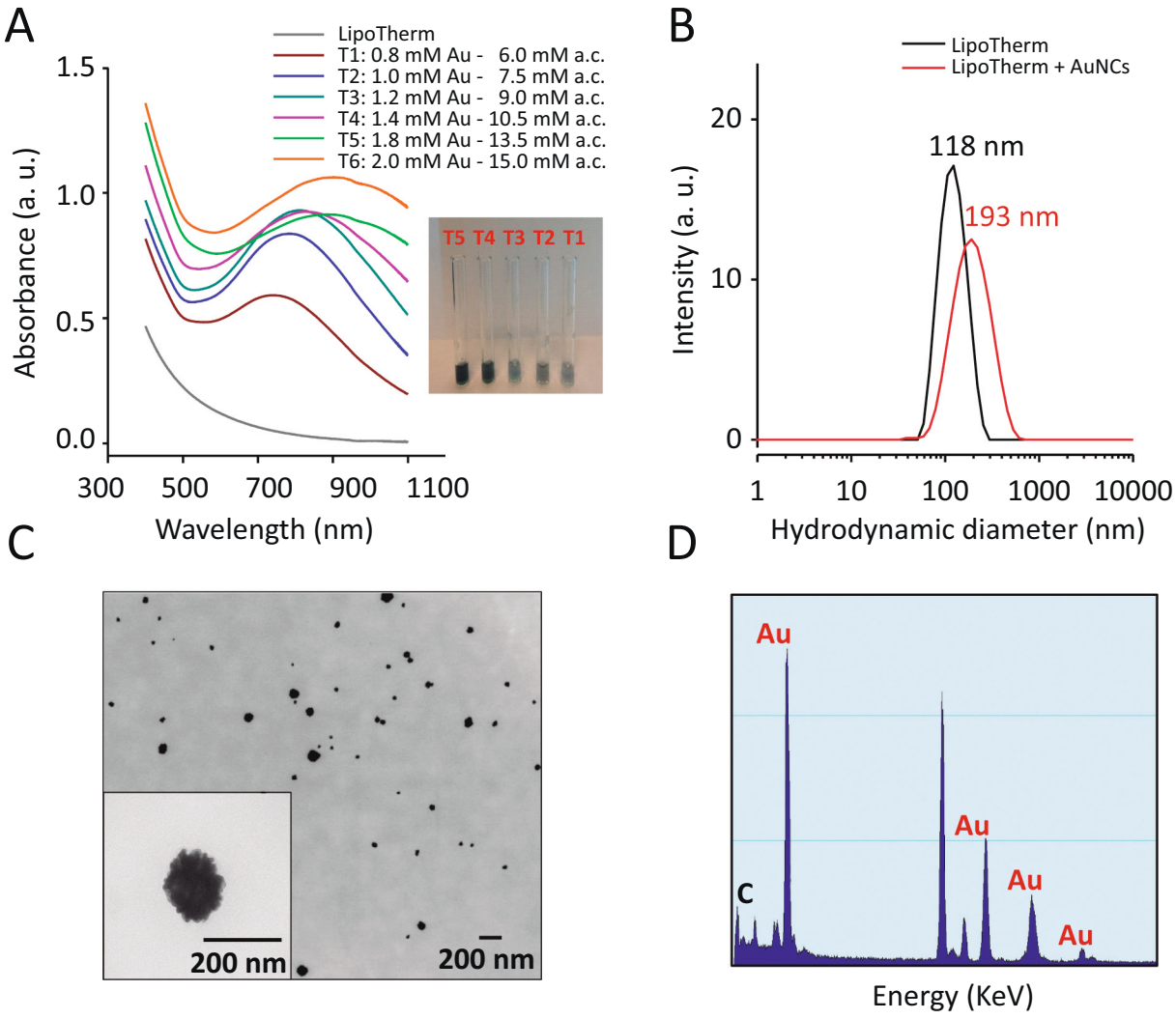

Fig. 5. Characterization of Ang-(1–9)-loaded LipoTherm-AuNC nanosystems. (A) UV–vis spectra of nanosystems with varying $HAuCl_4$ and ascorbic acid concentrations. (B) Dynamic light scattering (DLS) comparison of size distribution in the LipoTherm and Ang-(1–9)-loaded LipoTherm-AuNC nanosystems. (C) Transmission electron microscopy (TEM) images. (D) Chemical analysis of Ang-(1–9)-loaded LipoTherm-AuNC nanosystems by XEDS. Scale bars: 200 nm.

encapsulation into the aqueous core of the LipoTherm. Previous reports have indicated that liposome carriers can improve circulating times of short-lived peptides [28,29,51]. Angiotensin- [1–7] is another vasoactive peptide with a short blood half-life and its circulating times have been improved in liposomal formulations for brain administration [28,29]. Liposomes have also been used to enable efficacy of pulmonary acting peptides that exhibit a short half-life after local administration [51]. As such, vasoactive intestinal peptide has been encapsulated in liposomes to enhance its pulmonary bioavailability.

3.3. Temperature-dependent Ang-(1-9) release from LipoTherm

The release profiles of Ang-(1-9) from LipoTherm induced by temperature was evaluated for the three encapsulated concentrations (107, 153 and 183 μM). Fig. 4A shows the concentration of Ang-(1-9) released from the Lipotherm at T_m (43 °C) and body temperature (37 °C). Ang-(1–9)-loaded LipoTherm did not release a significant amount of Ang-(1-9) at 37 °C (around 1 μM), which demonstrated the stability of the loading inside the liposome cores, avoiding significant leakage at body temperature. Conversely, when the LipoTherm were exposed to 43 °C, Ang-(1-9) was released through the bilayer and the maximum released amount depended on the peptide concentration in the aqueous core. For instance, the maximum concentrations released at 10 min of heating were 40, 55 and 100 μM for the encapsulated loads of 107, 153 and 183 μM, respectively. These released amounts corresponded to 37%, 36% and 55% of their corresponding loads (Fig. 4B). These results showed that a higher Ang-(1-9) concentration loaded in the liposome aqueous core allows more Ang-(1-9) to pass through the lipid bilayer, by taking advantage of the lipid mobility and nanopores generated by the lysolipid (MSPC) at T_m [52]. Moreover, the release profiles were similar for all the drug payloads and these were characterized by a rapid release until 10 min; then, release reached a steady-state that lasted for the period studied. The transition from rapid to steady-state release was gradual between 5 and 10 min for the LipoTherm with 107 and 153 μM payloads, while this transition was sudden at 10 min for the 183 μM payload due to the higher Ang-(1-9) concentration inside the liposome core, which produced a faster diffusion through the bilayer. Similar drug release results have previously shown that temperatures higher than T_m are desired for a more complete and faster drug release from thermosensitive liposomes [53–55]. In this work, the release of Ang-(1-9) from the LipoTherm core was also favored by diluting Ang-(1-9) in a glucose solution to produce a higher inner osmotic pressure than that outside the liposome (PBS) [56]. Noteworthy, LipoTherm can release 100 μM of Ang-(1-9) after 10 min of heating, which has been reported as a therapeutic concentration in *in vitro* hypertrophy studies reported by Ocaranza et al. [11].

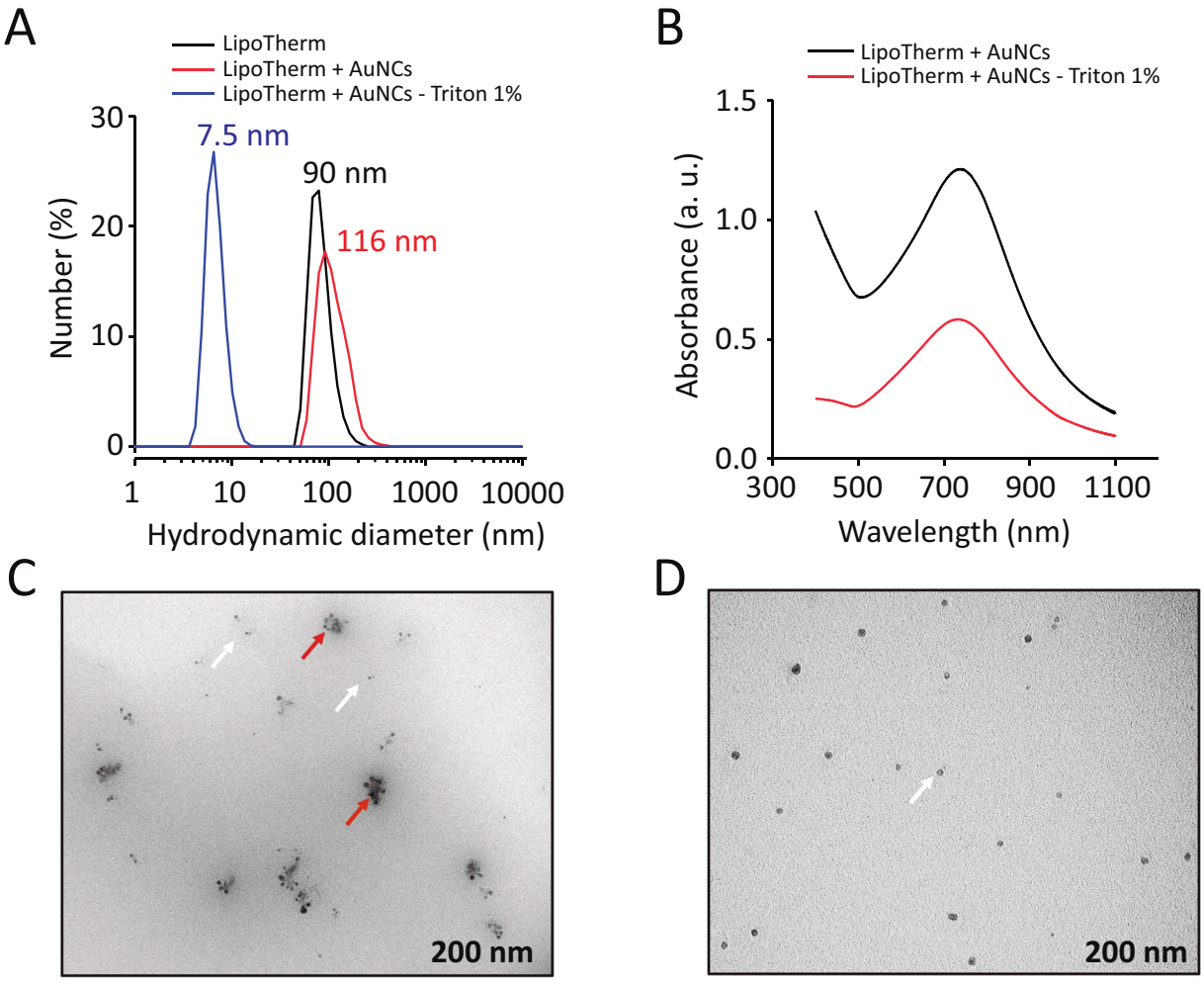

Fig. 6. Evaluation of Ang-(1–9)-loaded LipoTherm-AuNC nanosystem degradation after treatment with Triton X-100. (A) Dynamic light scattering (DLS) comparison of size distributions in LipoTherm, Ang-(1–9)-loaded LipoTherm-AuNC and Ang-(1–9)-loaded LipoTherm-AuNC nanosystems treated with 1% Triton X-100. (B) UV–vis absorption spectrum of Ang-(1–9)-loaded LipoTherm-AuNC and Ang-(1–9)-loaded LipoTherm-AuNC treated with 1% Triton X-100. (C-D) TEM images of Ang-(1–9)-loaded LipoTherm-AuNC nanosystem after treatment with 1% Triton X-100. Red arrows show gold nanoparticles attached to degraded LipoTherm and white arrows show independent gold nanoparticles. (For interpretation of the references to color in this figure legend, the reader is referred to the web version of this article.)

3.4. Ang-(1–9)-loaded LipoTherm-AuNC nanosystems

The synthesis of AuNC on the Ang-(1–9)-loaded LipoTherm outer surface and the characterization of the resulting nanosystems are shown in Fig. 5. The reduction of gold on the LipoTherm was evaluated by varying the concentrations of auric chloride and ascorbic acid, while the formation of AuNC was followed by measuring the absorption spectrum of the synthesized nanosystems (Fig. 5A). Before the gold reduction, LipoTherm only showed the short wavelength extinction due to the Rayleigh scattering of liposomes without any NIR absorption [38]. After using 0.8 mM of $HAuCl_4$ and 6 mM of ascorbic acid for the gold reduction (T1 synthesis), a NIR band between 600 nm and 1100 nm (maximum around 745 nm) was generated, thus showing the presence of gold nanoclusters coexisting with the liposomes. When higher concentrations of $HAuCl_4$ and ascorbic acid were used, the intensity of the NIR band increased and the maximum was shifted toward longer wavelengths for T2 (maximum around 780 nm) and T3 (maximum around 814 nm). However, when the concentrations of the reagents were even higher (T4, T5 and T6 synthesis), the bands became wider, indicating the formation of more polydisperse and denser gold nanostructures [38]. These synthetic conditions with larger amounts of $HAuCl_4$ and ascorbic acid showed a dark blue color, compared with the light blue obtained from the synthesis conditions with lower amounts of these reagents (Fig. 5A).

DLS was another technique used to evaluate gold reduction and choose optimal synthetic conditions. Fig. 5B shows the size distribution of both bare and gold-coated LipoTherm using the T1 synthesis condition. Before gold reduction, the LipoTherm showed an average size of 118 nm with low polydispersity (polydispersity index, PDI: 0.07), while after synthesis, the average size became 193 nm, with higher polydispersity (PDI: 0.20), thus confirming the formation of larger hybrid nanosystems composed of LipoTherm and gold nanostructures. Absence of other nanoparticle populations or large agglomerates was evidenced for T1 synthesis conditions (Fig. 5B). On the other hand, other nanoparticle populations with larger particle sizes (average particle size larger than 600 nm, depending on the gold concentration), probably composed of isolated AuNC or gold agglomerates not bound to the LipoTherm surface, or aggregations of AuNC and several liposomes were observed for the synthesis conditions with higher concentration of $HAuCl_4$ and ascorbic acid (see Supplementary Fig. 2). These DLS results showed that the T1 synthetic condition produces a more homogeneous LipoTherm-AuNC nanosystem.

The synthesized LipoTherm-AuNC nanosystem was also analyzed by TEM (Fig. 5C-D). The assembling of gold nanoparticles to form AuNC on

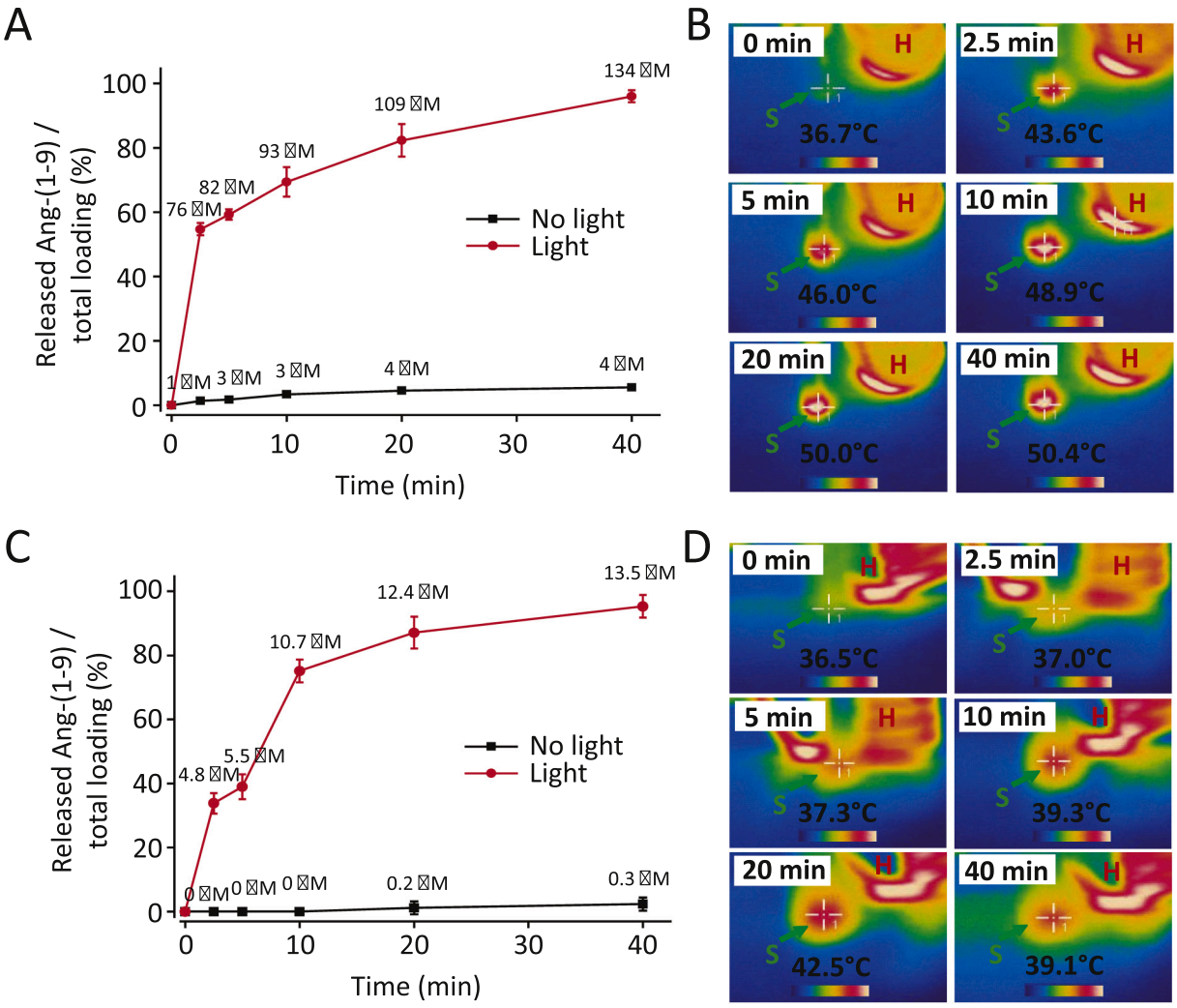

Fig. 7. Release of Ang-(1-9) and temperature changes after t1: 2.5 min, t2: 5 min, t3: 10 min, t4: 20 min and t5: 40 min of near-infrared (NIR) laser irradiation of Ang-(1–9)-loaded LipoTherm-AuNC nanosystem. (A) Ang-(1-9) release profile. (B) Thermal images after irradiation of the nanosystem, as synthesized. (C) Ang-(1-9) release profile. (D) Thermal images after irradiation of the nanosystem, diluted ten times.

the LipoTherm was confirmed (Fig. 5C), as the large number of high-contrast nanoparticles covering the LipoTherm was evident. Furthermore, a compositional analysis by XEDS confirmed that these nanoclusters were made of gold (Fig. 5D). These AuNC surrounding the LipoTherm were composed of gold nanoparticles with sizes around 10 nm (TEM image magnified in Fig. 5C) and the resulting Ang-(1–9)-loaded LipoThem-AuNC nanosystems showed particle sizes consistent with the range of sizes obtained from the DLS analysis (Fig. 5B). The collective plasmon resonance depends on the number of the gold nanoparticles that are part of the AuNC and the nanocomposite formed with the lipid bilayer [38,57].

3.5. Disintegration of the AuNC after LipoTherm degradation

Clearance of nanoparticles used for treatment or diagnosis remains a major challenge [38]. The LipoTherm-AuNC nanosystem was designed to absorb NIR radiation (a preferred spectral range for irradiation due to its weak interaction with biological tissue), release its cargo and finally degrade in organic molecules and inorganic components around 5 nm to facilitate their renal elimination [38,58]. Fig. 6A shows evidence of the Ang-(1–9)-loaded LipoTherm-AuNC nanosystem degradation after the treatment with 1% Triton X100, condition in which the average size of the nanosystem decreased from 116 nm to 7.5 nm (ranged from 2.5 to 20 nm), indicating that the disruption/lysis of the liposomes further promoted AuNC disintegration. The degradation of this nanosystem was also evaluated by measuring the absorption spectrum before and after the treatment with Triton X-100 (Fig. 6B). After the Triton X-100 treatment, the nanosystem showed a NIR absorption spectrum with a lower intensity than that from the pristine nanosystem before the treatment. Moreover, the UV absorption from the liposomes at wavelengths below 500 nm markedly decreased after the treatment. Optical density or turbidity is mainly affected by the number and size of the particles present in a dispersion; hence, if the number of liposomes or their size is reduced, the absorbed UV light decreases accordingly [59,60]. Therefore, this UV–vis result in Fig. 6B indicates that the liposomes were disrupted or degraded by the Triton X-100 treatment. The residual NIR absorption on this same spectrum suggests that there are still AuNC forming more stable shells, which did not disintegrate when the liposome was degraded. The disintegration of the nanosystem was confirmed by TEM (Fig. 6C-D). Liposomal debris or deformed liposomes grouped with some disaggregated gold nanoparticles were observed and indicated with the red arrows in Fig. 6C. Gold nanoparticles were completely disaggregated and isolated, showing sizes between 4 and 15 nm, approximately (white arrows in Fig. 6C-D). These particle sizes observed by TEM were consistent with the particle size distribution obtained by DLS (Fig. 6A), thus confirming the potential for renal

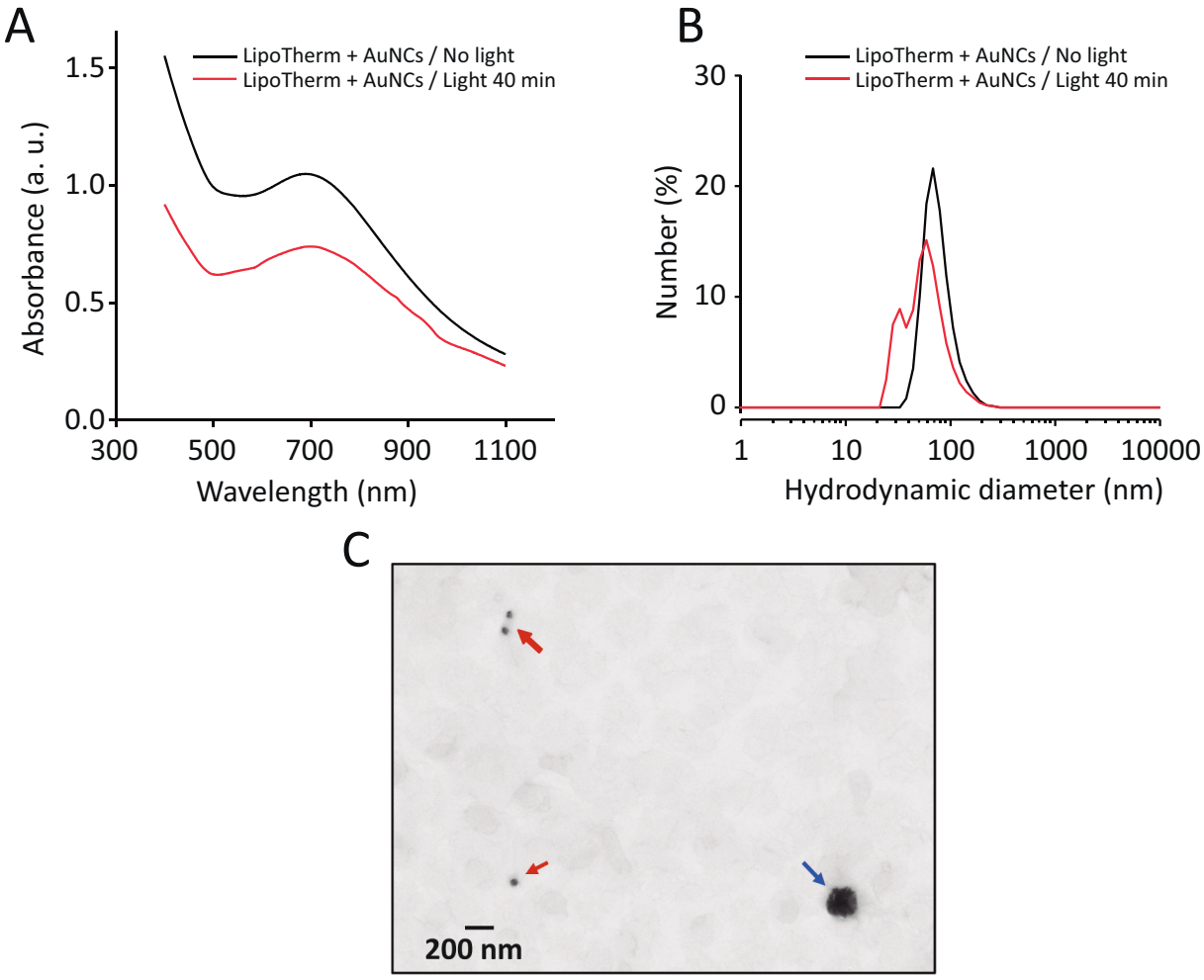

Fig. 8. Evaluation of the effect of laser irradiation on the LipoTherm-AuNC nanosystem. (A) UV–vis spectrum. (B) Size distribution by dynamic light scattering (DLS). (C) Transmission electron microscopy (TEM) images of the nanosystem after 40 min of laser irradiation. Bar scale: 200 nm.

elimination of the Ang-(1–9)-loaded LipoTherm-AuNC nanosystem, as was reported for quantum dots smaller than 6 nm [58]. Troutman et al. [38] also showed that the disintegration of gold nanoshells/DPPC liposome nanosystems generates small gold nanoparticles which can be potentially eliminated by the renal system. In this study, the complete disintegration of the nanosystem was obtained with the surfactant Triton X-100. Additionally, the same level of degradation could be achieved under conditions representing a biologically relevant process by means of a lipid hydrolysis model produced by phospholipase A2 (PLA2) in the presence of calcium (physiologic pathway of lipid breakdown and recycling).

3.6. NIR-activated Ang-(1-9) release from the LipoTherm-AuNC nanosystem

The controlled release of Ang-(1-9) from the Ang-(1–9)-loaded LipoTherm-AuNC nanosystem was evaluated using NIR laser irradiation as an external stimulus. Fig. 7 shows the percentage and concentration of Ang-(1-9) released after 2.5, 5, 10, 20 and 40 min of laser irradiation, as well as the thermal images representing the temperature changes in the nanosystem dispersion during the irradiation. Fig. 7A-B depicts the release from the nanosystem sample without dilution; *i.e.*, at the same nanoparticle concentration as that synthesized. Meanwhile, Fig. 7C-D represents a ten times-diluted sample, as used for the cell test.

The nanosystem, maintained at about 37 °C under stirring, showed a maximum Ang-(1-9) release of around 5% (4 μM) of the total peptide load until 40 min. This small quantity of released Ang-(1-9) could be associated with Ang-(1-9) remaining over the nanosystem surface or passive diffusion of Ang-(1-9) through the lipid bilayer over time. Laser stimulation for 2.5 min led to a fast release of around 55% (76 μM) of Ang-(1-9) during this early irradiation period. The sample irradiated for 10 min released 70% of the initial encapsulated Ang-(1-9). The Ang-(1-9) amount released from the nanosystem increased with irradiation time, until reaching a release of 96% after 40 min of irradiation. It is worth pointing out that when the LipoTherm (non coated with AuNC) was heated using a water bath for 40 min, the percentages of released Ang-(1-9) were lesser (33%–53%) (Fig. 4) that the light-induced release at the same time point. It is believed that the hyperthermia and physical effect produced by the the NIR irradiation of AuNC generated a more effective Ang-(1-9) release from the LipoTherm due to either a higher local temperature or formation and collapse of vapor bubbles around the laser-heated AuNC, similar to a transient cavitation effect [33]. The temperature of the nanosystem samples also increased with irradiation time from approximately 37 °C up to around 50 °C at 40 min (Fig. 7B). These thermal images helped to monitor the temperature of the surrounding medium at each irradiation time; therefore, the temperatures shown in Fig. 7B indicated that this concentration of the AuNC-LipoTherm nanosystem was not safe for the cells or tissue. Therefore, the light-induced Ang-(1-9) release and the associated temperature changes were also evaluated using a ten-fold diluted sample (Fig. 7C-D). The release profile of this diluted sample was slightly different at early times (2.5 and 5 min) from that of the non-diluted sample, showing a

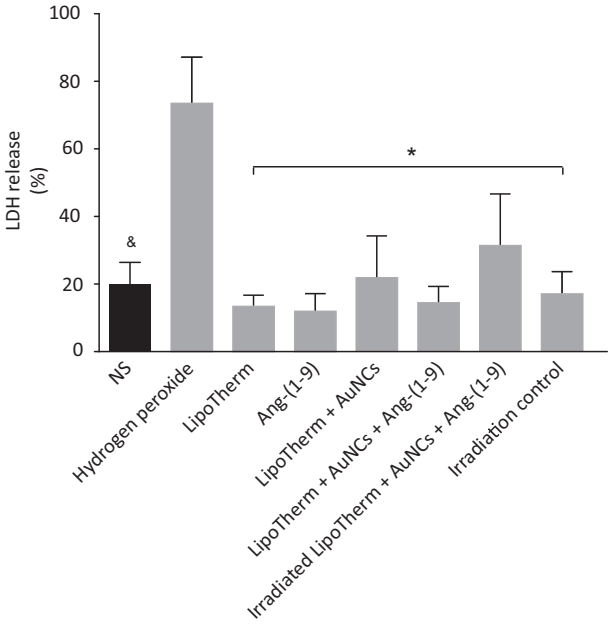

Fig. 9. LDH cytotoxicity test to evaluate the effect of the Ang-(1–9)-loaded LipoTherm-AuNC nanosystem and the NIR irradiation conditions on cardiomyocytes. The graph shows the percentage (%) of lactate dehydrogenase (LDH) released into the culture medium after incubation with the different treatments. Data is expressed as mean ± SEM. Sample size of 5 independent experiments. Data were analyzed by 2-way Kruskal-Wallis test, and Dunn's Multiple Comparison post-analysis. $^{\&}p < 0.005$ *vs* positive control (H_2O_2), $^{*}p < 0.05$ *vs* positive control (H_2O_2).

smaller Ang-(1-9) release from the nanosystem due to the lower temperature generated in the dispersion (37 °C) or around the liposomes. Therefore, the non-diluted sample (43 °C-46 °C) probably did not allow adequate bilayer permeabilization at earlier times. The release at times longer than 10 min had a behaviour comparable to that of the non-diluted sample, showing similar percentages of released Ang-(1-9). Moreover, the concentration of the released Ang-(1-9) was consistent with the dilution factor. This diluted sample generated lower and safer temperatures for cells or surrounding tissue (Fig. 7D). Similar release profiles for gold-functionalized thermal-liposomes have been previously described [48,55]. Over short periods of time of continued laser irradiation (min range), much of the drug payload is quickly released, enabling its triggerable release.

3.7. Effect of hyperthermia on the LipoTherm-AuNC nanosystem

The effect of hyperthermia on the LipoTherm-AuNC nanosystem after laser irradiation was evaluated by UV–vis spectrophotometry, DLS and TEM (Fig. 8). After 40 min of irradiation, the nanosystem showed a NIR absorption spectrum with lower intensity, compared to that of the nanosystem without irradiation (Fig. 8A). The size distribution showed a change in the nanoparticle population after irradiation, generating a distribution with a higher polydispersity and an additional nanoparticle population of smaller sizes (Fig. 8B). These results from UV–vis spectrophotometry and DLS could indicatesuggest that these AuNC-based nanosystems suffered morphological changes and AuNC disaggregation, possibly due possibly to the effect of localized high temperatures and physical phenomena suffered byon the AuNC during NIR illumination [33,61]. TEM images (Fig. 8C) obtained from the irradiated samples supported revealed the dissaggregation of the AuNC-based nanosystems as nanoparticles with typical morphology and sizes (indicated by blue arrows), along with some smaller isolated gold nanoparticles of around 20 nm (indicated by red arrows) were observed. We were not able to detect many of these smaller AuNC or gold nanoparticles by TEM. However, these evaluations (UV–vis, DLS, and TEM) indicated that NIR irradiation induces some morphological changes of the nanosystems.

3.8. Cell viability

The cytotoxic effect of the Ang-(1–9)-loaded LipoTherm-AuNC nanosystems on NRVM was investigated after 24 h. Fig. 9 shows that there was no significant cytotoxic effect of the LipoTherm-AuNC nanosystems, compared to the negative control (No stimulus, NS). Bare LipoTherm and Ang-(1-9) were also evaluated as controls. Moreover, no cytotoxic effect was detected after laser illumination of the Ang-(1–9)-loaded LipoTherm-AuNC nanosystem (ten times diluted) for 10 min. This result shows that the increase in temperature generated by the laser irradiation did not produce cardiomyocyte toxicity. In conclusion, the Ang-(1–9)-loaded LipoTherm-AuNC nanosystem at the indicated concentrations and NIR irradiation conditions did not produce significant effects on cell viability.

3.9. Cardiac function measurements after administration of Ang-(1–9)-loaded LipoTherm-AuNC

With the purpose of evaluating if Ang-(1-9) released from the LipoTherm-AuNC nanosystem after NIR illumination still retained its biological activity in the heart, the Langendorff model was used to study *ex vivo* myocardial function after administration of the released Ang-(1-9).

Ang-(1–9)-loaded LipoTherm-AuNC improved left ventricular function in isolated adult rat hearts and are biologically compatible with isolated hearts, in a manner similar to that reported by Mendoza-Torres *et al* [62]. As shown in Fig. 10, treatment with 0.5 nM Ang-(1-9) released post irradiation (laser 808 nm, 350 mW for 10 min) from loaded LipoTherm-AuNC Lipo-Au-Ang) during perfusion, improved LVDP by approximately 17%, compared to the negative control (empty LipoTherm-AuNC post irradiation, Lipo-Au). Importantly, this result depicts that the Ang-(1–9)-loaded LipoTherm-AuNC nanosystem at this Ang-(1-9) concentration and NIR irradiation conditions is able to generate a significant pharmacological effect in isolated adult rat hearts, showing that the light-induced release of Ang-(1-9) from the LipoTherm-AuNC nanosystem did not affect its biological activity.

This study shows the temporal controlled release capacity achieved by NIR irradiation. Our research group is working on novel active targeting strategies to provide spatially controlled release of the Ang-(1–9)-loaded LipoTherm-AuNC nanosystem. This approach would generate a nanosystem able to release Ang-(1-9) at a specific area at the desired time. Moreover, it would allow taking better advantage of the therapeutic effects of this peptide.

Future clinical applications of this technology should explore any of the current approaches used for cardiac laser revascularization. In this case, a commercial NIR laser fiber could be inserted using either transmyocardial or percutaneous procedures. The transmyocardial procedure consists in creating a small incision between the ribs (thoracotomy) with the patient under general anesthesia. Then, the flexible laser fiber is positioned on the surface of the beating heart. In the percutaneous procedure, the surgeon injects a local anesthetic into an area on the groin and then makes a tiny incision to place a catheter in the femoral artery. A fiber-optic catheter is then placed inside the first catheter and guided through the blood vessels to the heart [63,64].

4. Conclusions

In this work, a thermo-sensitive LipoTherm-AuNC nanosystem was developed to enable NIR-triggered Ang-(1-9) release. MSPC and DSPC incorporation in the DPPC liposomal system allowed the effective release of the Ang-(1-9) peptide with a precise release control by thermal stimulation at T_m. Ang-(1-9) was appropriately protected from

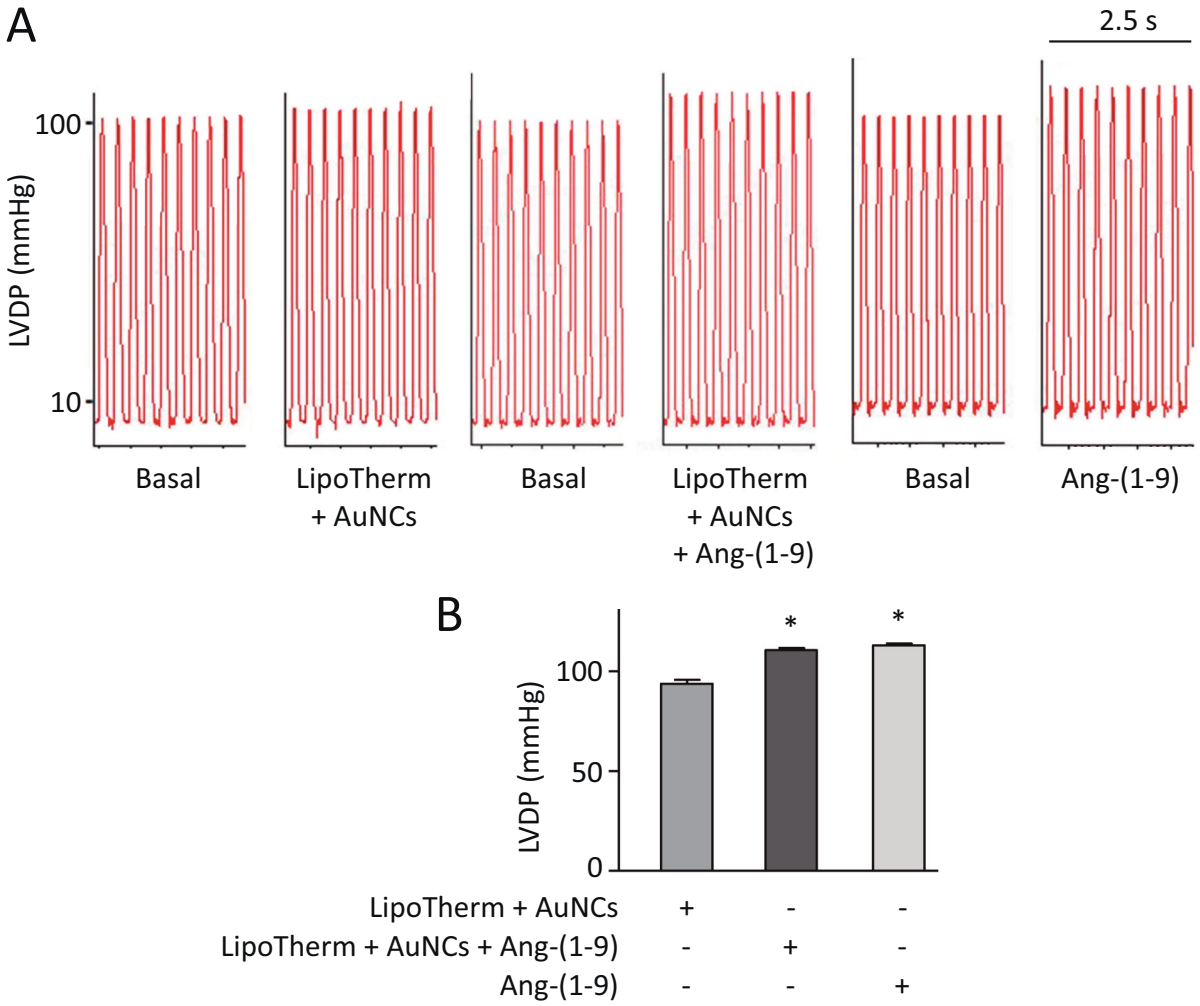

Fig. 10. Effect of the Ang-(1–9)-loaded LipoTherm-AuNC nanosystem on myocardial function using the Langendorff model. (A) Representative tracings of LVDP at 2.5 s after treatment with respect to baseline. (B) LVDP measured at 2.5 s after treatments. Bar graphs represent mean ± SEM. $N = 7$ hearts in each condition. *$p < 0.05$ *vs* control hearts with LipoTherm + AuNCs. Data were analyzed by 2-way Kruskal-Wallis test and Dunn's Multiple Comparison post-analysis. LVDP: left ventricular developed pressure; LipoTherm + AuNCs: supernatant from irradiated LipoTherm-AuNC nanosystem; LipoTherm + AuNCs + Ang-(1-9): supernatant from irradiated Ang-(1–9)-loaded LipoTherm-AuNC nanosystem.

enzymatic degradation in the nanosystems and revealed a triggered release upon NIR irradiation, releasing its complete payload during the time period of this study. Ang-(1–9)-loaded LipoTherm-AuNC nanosystems were safe in both the *in vitro* cell testing and the *ex vivo* Langendorff heart model. Moreover, the released Ang-(1-9)from this nanosystem elicited improved LVDP. These results reveal the potential of the triggerable system for -the otherwise short-lived- Ang-(1-9) as an enabler of its pharmacological effect. For future *in vivo* studies and clinical practice, it would be interesting to the evaluate pulsed NIR sources with micro-, nano-, pico- or femtosecond pulses, which have shown efficient localized stimulation of nanosystems, therefore achieving the release of the content with minimal or no thermal impact to the surrounding tissue.

Declaration of Competing Interest

Drs. Ocaranza, Chiong and Lavandero are coinventors on the patent US9,511,120 (December 6, 2016). The patent relates to the actions of angiotensin-(1-9) on hypertension and cardiovascular remodeling. The other authors declare that they have no known competing financial interests or personal relationships that could have appeared to influence the work reported in this paper.

Acknowledgments

The authors received funding from Agencia Nacional de Investigación y Desarrollo (ANID), Chile: grants FONDAP 15130011 (to M.P. O., J.A.R., M.C., M.K. and S.L); Puente Pontificia Universidad Católica de Chile (033/2020 to M.P.O.), Fondecyt 1190623 (E.A) and 1200490 (to S.L.), Bayer AG (Program Grants4Targets ID 2017-08-2260 (to M.P. O., M.C. and S.L.), Anillo ACT192144 (to M.P.O., E.A, and J.M.), Fondecyt Postdoctoral Fellowship 3160323 (J.B) and FONDEQUIP EQM160157 and EQM170111.

Appendix A. Supplementary data

Supplementary data to this article can be found online at https://doi.org/10.1016/j.jconrel.2020.11.002.

References

[1] World Health Organization, Media Centre: Cardiovascular Disease. http://www.who.int/mediacentre/factsheets/fs317/en/.
[2] T.M. Coffman, Under pressure: the search for the essential mechanisms of hypertension, Nat. Med. 17 (2011) 1402–1409.
[3] E.J. Benjamin, M.J. Blaha, S.E. Chiuve, M. Cushman, S.R. Das, R. Deo, S.D. de Ferranti, J. Floyd, M. Fornage, C. Gillespie, C.R. Isasi, M.C. Jimenez, L.C. Jordan, S.

E. Judd, D. Lackland, J.H. Lichtman, L. Lisabeth, S. Liu, C.T. Longenecker, R. H. Mackey, K. Matsushita, D. Mozaffarian, M.E. Mussolino, K. Nasir, R.W. Neumar, L. Palaniappan, D.K. Pandey, R.R. Thiagarajan, M.J. Reeves, M. Ritchey, C. J. Rodriguez, G.A. Roth, W.D. Rosamond, C. Sasson, A. Towfighi, C.W. Tsao, M. B. Turner, S.S. Virani, J.H. Voeks, J.Z. Willey, J.T. Wilkins, J.H. Wu, H.M. Alger, S. S. Wong, P. Muntner, C. American Heart Association Statistics, S. Stroke Statistics, Heart Disease and Stroke Statistics-2017 Update: A report from the American Heart Association, Circulation 135 (2017) e146–e603.

[4] E. Mendoza-Torres, A. Oyarzun, D. Mondaca-Ruff, A. Azocar, P.F. Castro, J.E. Jalil, M. Chiong, S. Lavandero, M.P. Ocaranza, ACE2 and vasoactive peptides: novel players in cardiovascular/renal remodeling and hypertension, Ther. Adv. Cardiovasc. Dis. 9 (2015) 217–237.

[5] F. Westermeier, M. Bustamante, M. Pavez, L. Garcia, M. Chiong, M.P. Ocaranza, S. Lavandero, Novel players in cardioprotection: insulin like growth factor-1, angiotensin-(1-7) and angiotensin-(1-9), Pharmacol. Res. 101 (2015) 41–55.

[6] C.A. McKinney, C. Fattah, C.M. Loughrey, G. Milligan, S.A. Nicklin, Angiotensin-(1-7) and angiotensin-(1-9): function in cardiac and vascular remodelling, Clin. Sci. (Lond.) 126 (2014) 815–827.

[7] M.P. Ocaranza, L. Michea, M. Chiong, C.F. Lagos, S. Lavandero, J.E. Jalil, Recent insights and therapeutic perspectives of angiotensin-(1-9) in the cardiovascular system, Clin. Sci. (Lond.) 127 (2014) 549–557.

[8] L.M. Delbridge, L.A. Bienvenu, K.M. Mellor, Angiotensin-(1-9): new promise for post-infarct functional therapy, J. Am. Coll. Cardiol. 68 (2016) 2667–2669.

[9] M. Paz Ocaranza, J.A. Riquelme, L. García, J.E. Jalil, M. Chiong, R.A.S. Santos, S. Lavandero, Counter-regulatory renin-angiotensin system in cardiovascular disease, Nat. Rev. Cardiol. 17 (2020) 116–129.

[10] M. Flores-Munoz, L.M. Work, K. Douglas, L. Denby, A.F. Dominiczak, D. Graham, S. A. Nicklin, Angiotensin-(1-9) attenuates cardiac fibrosis in the stroke-prone spontaneously hypertensive rat via the angiotensin type 2 receptor, Hypertension 59 (2012) 300–307.

[11] M.P. Ocaranza, S. Lavandero, J.E. Jalil, J. Moya, M. Pinto, U. Novoa, F. Apablaza, L. Gonzalez, C. Hernandez, M. Varas, R. Lopez, I. Godoy, H. Verdejo, M. Chiong, Angiotensin-(1-9) regulates cardiac hypertrophy in vivo and in vitro, J. Hypertens. 28 (2010) 1054–1064.

[12] M.P. Ocaranza, J. Moya, V. Barrientos, R. Alzamora, D. Hevia, C. Morales, M. Pinto, N. Escudero, L. Garcia, U. Novoa, P. Ayala, G. Diaz-Araya, I. Godoy, M. Chiong, S. Lavandero, J.E. Jalil, L. Michea, Angiotensin-(1-9) reverses experimental hypertension and cardiovascular damage by inhibition of the angiotensin converting enzyme/Ang II axis, J. Hypertens. 32 (2014) 771–783.

[13] M. Flores-Munoz, N.J. Smith, C. Haggerty, G. Milligan, S.A. Nicklin, Angiotensin1-9 antagonises pro-hypertrophic signalling in cardiomyocytes via the angiotensin type 2 receptor, J. Physiol. 589 (2011) 939–951.

[14] C. Fattah, K. Nather, C.S. McCarroll, M.P. Hortigon-Vinagre, V. Zamora, M. Flores-Munoz, L. McArthur, L. Zentilin, M. Giacca, R.M. Touyz, G.L. Smith, C. M. Loughrey, S.A. Nicklin, Gene therapy with angiotensin-(1-9) preserves left ventricular systolic function after myocardial infarction, J. Am. Coll. Cardiol. 68 (2016) 2652–2666.

[15] Z. Chen, F. Tan, E.G. Erdös, P.A. Deddish, Hydrolysis of angiotensin peptides by human angiotensin I–converting enzyme and the resensitization of B₂ kinin receptors, Hypertension 46 (2005) 1368–1373.

[16] L. Gonzalez, U. Novoa, J. Moya, L. Gabrielli, J.E. Jalil, L. Garcia, M. Chiong, S. Lavandero, M.P. Ocaranza, Angiotensin-(1-9) reduces cardiovascular and renal inflammation in experimental renin-independent hypertension, Biochem. Pharmacol. 156 (2018) 357–370.

[17] F. Jiang, J. Yang, Y. Zhang, M. Dong, S. Wang, Q. Zhang, F.F. Liu, K. Zhang, C. Zhang, Angiotensin-converting enzyme 2 and angiotensin 1-7: novel therapeutic targets, Nat. Rev. Cardiol. 11 (2014) 413–426.

[18] G.U. Ruiz-Esparza, J.H. Flores-Arredondo, V. Segura-Ibarra, G. Torre-Amione, M. Ferrari, E. Blanco, R.E. Serda, The physiology of cardiovascular disease and innovative liposomal platforms for therapy, Int. J. Nanomedicine 8 (2013) 629–640.

[19] L. Brito, M. Amiji, Nanoparticulate carriers for the treatment of coronary restenosis, Int. J. Nanomedicine 2 (2007) 143–161.

[20] I. Cicha, D. Garlichs Christoph, C. Alexiou, Cardiovascular therapy through nanotechnology – how far are we still from bedside? Eur. J. Nanomed. (2014) 63.

[21] B. Singh, T. Garg, A.K. Goyal, G. Rath, Recent advancements in the cardiovascular drug carriers, Artif. Cells Nanomed. Biotechnol. 44 (2016) 216–225.

[22] H. Takahama, T. Minamino, H. Asanuma, M. Fujita, T. Asai, M. Wakeno, H. Sasaki, H. Kikuchi, K. Hashimoto, N. Oku, M. Asakura, J. Kim, S. Takashima, K. Komamura, M. Sugimachi, N. Mochizuki, M. Kitakaze, Prolonged targeting of ischemic/reperfused myocardium by liposomal adenosine augments cardioprotection in rats, J. Am. Coll. Cardiol. 53 (2009) 709–717.

[23] K. Ichimura, T. Matoba, K. Nakano, M. Tokutome, K. Honda, J.-i. Koga, K. Egashira, A translational study of a new therapeutic approach for acute myocardial infarction: nanoparticle-mediated delivery of Pitavastatin into Reperfused myocardium reduces ischemia-reperfusion injury in a preclinical porcine model, PLoS One 11 (2016), e0162425.

[24] V. Serpooshan, S. Sivanesan, X. Huang, M. Mahmoudi, A.V. Malkovskiy, M. Zhao, M. Inayathullah, D. Wagh, X.J. Zhang, S. Metzler, D. Bernstein, J.C. Wu, P. Ruiz-Lozano, J. Rajadas, [Pyr1]-Apelin-13 delivery via nano-liposomal encapsulation attenuates pressure overload-induced cardiac dysfunction, Biomaterials 37 (2015) 289–298.

[25] K. Bowey, J.F. Tanguay, M. Tabrizian, Liposome technology for cardiovascular disease treatment and diagnosis, Expert Opin. Drug Deliv. 9 (2012) 249–265.

[26] I.E. Allijn, B.M.S. Czarny, X. Wang, S.Y. Chong, M. Weiler, A.E. da Silva, J. M. Metselaar, C.S.P. Lam, G. Pastorin, D.P.V. de Kleijn, G. Storm, J.W. Wang, R. M. Schiffelers, Liposome encapsulated berberine treatment attenuates cardiac dysfunction after myocardial infarction, J. Control. Release 247 (2017) 127–133.

[27] S.S.K. Dasa, R. Suzuki, M. Gutknecht, L.T. Brinton, Y. Tian, E. Michaelsson, L. Lindfors, A.L. Klibanov, B.A. French, K.A. Kelly, Development of target-specific liposomes for delivering small molecule drugs after reperfused myocardial infarction, J. Control. Release 220 (2015) 556–567.

[28] N.M. Silva-Barcellos, S. Caligiorne, R.A.S. dos Santos, F. Frézard, Site-specific microinjection of liposomes into the brain for local infusion of a short-lived peptide, J. Control. Release 95 (2004) 301–307.

[29] N.M. Silva-Barcellos, F. Frézard, S. Caligiorne, R.A.S. Santos, Long-lasting cardiovascular effects of liposome-entrapped angiotensin-(1-7) at the rostral ventrolateral medulla, Hypertension 38 (2001) 1266–1271.

[30] A.K. Deshantri, A. Varela Moreira, V. Ecker, S.N. Mandhane, R.M. Schiffelers, M. Buchner, M.H.A.M. Fens, Nanomedicines for the treatment of hematological malignancies, J. Control. Release 287 (2018) 194–215.

[31] M. Abri Aghdam, R. Bagheri, J. Mosafer, B. Baradaran, M. Hashemzaei, A. Baghbanzadeh, M. de la Guardia, A. Mokhtarzadeh, Recent advances on thermosensitive and pH-sensitive liposomes employed in controlled release, J. Control. Release 315 (2019) 1–22.

[32] H. He, D. Yuan, Y. Wu, Y. Cao, Pharmacokinetics and pharmacodynamics modeling and simulation systems to support the development and regulation of liposomal drugs, Pharmaceutics 11 (2019).

[33] G. Wu, A. Mikhailovsky, H.A. Khant, C. Fu, W. Chiu, J.A. Zasadzinski, Remotely triggered liposome release by near-infrared light absorption via hollow gold nanoshells, J. Am. Chem. Soc. 130 (2008) 8175–8177.

[34] A. Mueller, B. Bondurant, D.F. O'Brien, Visible-light-stimulated destabilization of PEG-liposomes, Macromolecules 33 (2000) 4799–4804.

[35] B. Kneidl, M. Peller, G. Winter, L.H. Lindner, M. Hossann, Thermosensitive liposomal drug delivery systems: state of the art review, Int. J. Nanomedicine 9 (2014) 4387–4398.

[36] J.K. Mills, D. Needham, Lysolipid incorporation in dipalmitoylphosphatidylcholine bilayer membranes enhances the ion permeability and drug release rates at the membrane phase transition, Biochim. Biophys. Acta Biomembr. 1716 (2005) 77–96.

[37] S.J. Leung, T.S. Troutman, M. Romanowski, Plasmon resonant gold-coated liposomes for spectrally coded content release, Proc. SPIE Int. Soc. Opt. Eng. 7190 (2009).

[38] T.S. Troutman, J.K. Barton, M. Romanowski, Biodegradable Plasmon Resonant Nanoshells, Adv. Mater. 20 (2008) 2604–2608.

[39] T.S. Troutman, S.J. Leung, M. Romanowski, Light-induced content release from Plasmon resonant liposomes, Adv. Mater. 21 (2009) 2334–2338.

[40] S.J. Leung, M. Romanowski, Light-activated content release from liposomes, Theranostics 2 (2012) 1020–1036.

[41] T.J.T.P. van den Berg, H. Spekreijse, Near infrared light absorption in the human eye media, Vis. Res. 37 (1997) 249–253.

[42] K. Sandhya, B. Ravindranath, A protocol for racemization-free loading of Fmoc-amino acids to Wang resin, Tetrahedron Lett. 49 (2008) 2435–2437.

[43] T. Tagami, J.P. May, M.J. Ernsting, S.-D. Li, A thermosensitive liposome prepared with a Cu^{2+} gradient demonstrates improved pharmacokinetics, drug delivery and antitumor efficacy, J. Control. Release 161 (2012) 142–149.

[44] S.J. Leung, X.M. Kachur, M.C. Bobnick, M. Romanowski, Wavelength-selective light-induced release from Plasmon resonant liposomes, Adv. Funct. Mater. 21 (2011) 1113–1121.

[45] R. Foncea, M. Andersson, A. Ketterman, V. Blakesley, M. Sapag-Hagar, P. H. Sugden, D. LeRoith, S. Lavandero, Insulin-like growth factor-I rapidly activates multiple signal transduction pathways in cultured rat cardiac myocytes, J. Biol. Chem. 272 (1997) 19115–19124.

[46] R.M. Bell, M.M. Mocanu, D.M. Yellon, Retrograde heart perfusion: the Langendorff technique of isolated heart perfusion, J. Mol. Cell. Cardiol. 50 (2011) 940–950.

[47] M. Hossann, T. Wang, M. Wiggenhorn, R. Schmidt, A. Zengerle, G. Winter, H. Eibl, M. Peller, M. Reiser, R.D. Issels, L.H. Lindner, Size of thermosensitive liposomes influences content release, J. Control. Release 147 (2010) 436–443.

[48] J. Chen, C.Q. He, A.H. Lin, W. Gu, Z.P. Chen, W. Li, B.C. Cai, Thermosensitive liposomes with higher phase transition temperature for targeted drug delivery to tumor, Int. J. Pharm. 475 (2014) 408–415.

[49] D. Zucker, D. Marcus, Y. Barenholz, A. Goldblum, Liposome drugs' loading efficiency: a working model based on loading conditions and drug's physicochemical properties, J. Control. Release 139 (2009) 73–80.

[50] N. Kittana, Angiotensin-converting enzyme 2-angiotensin 1-7/1-9 system: novel promising targets for heart failure treatment, Fundam. Clin. Pharmacol. 32 (2018) 14–25.

[51] F. Hajos, B. Stark, S. Hensler, R. Prassl, W. Mosgoeller, Inhalable liposomal formulation for vasoactive intestinal peptide, Int. J. Pharm. 357 (2008) 286–294.

[52] D. Needham, J.Y. Park, A.M. Wright, J. Tong, Materials characterization of the low temperature sensitive liposome (LTSL): effects of the lipid composition (lysolipid and DSPE-PEG2000) on the thermal transition and release of doxorubicin, Faraday Discuss. 161 (2013) 515–534 (discussion 563-589).

[53] Y. Liu, X. Zhang, L. Luo, L. Li, Y. He, J. An, D. Gao, Self-assembly of stimuli-responsive au–Pd bimetallic Nanoflowers based on Betulinic acid liposomes for synergistic chemo-Photothermal Cancer therapy, ACS Biomater. Sci. Eng. 4 (2018) 2911–2921.

[54] Y. Liu, X. Zhang, L. Luo, L. Li, R.Y. Zhu, A. Li, Y. He, W. Cao, K. Niu, H. Liu, J. Yang, D. Gao, Gold-nanobranched-shell based drug vehicles with ultrahigh photothermal efficiency for chemo-photothermal therapy, Nanomedicine 18 (2019) 303–314.

[55] D. Apicella, M. Arruebo, R. Campardelli, M. Encabo Berzosa, P. Trucillo, V. Sebastian, J. Santamaria, E. Reverchon, Efficient gram-scale continuous

production of near-infrared-sensitive liposomes for light-triggered delivery of polyinosinic-polycytidylic acid, Chem. Eng. Process. Process Intensif. 146 (2019) 107709.
[56] N. Oku, R. Naruse, K. Doi, S. Okada, Potential usage of thermosensitive liposomes for macromolecule delivery, Biochim. Biophys. Acta Biomembr. 1191 (1994) 389–391.
[57] S.J. Leung, M. Romanowski, Molecular catch and release: controlled delivery using optical trapping with light-responsive liposomes, Adv. Mater. 24 (2012) 6380–6383.
[58] H.S. Choi, W. Liu, P. Misra, E. Tanaka, J.P. Zimmer, B. Itty Ipe, M.G. Bawendi, J. V. Frangioni, Renal clearance of quantum dots, Nat. Biotechnol. 25 (2007) 1165–1170.
[59] G.F. Lothian, F.P. Chappel, The transmission of light through suspensions, J. Appl. Chem. 1 (1951) 475–482.
[60] T. Radomirovic, P. Smith, F. Jones, Using absorbance as a measure of turbidity in highly caustic solutions, Int. J. Miner. Process. 118 (2013) 59–64.
[61] G. Wu, A. Mikhailovsky, H.A. Khant, J.A. Zasadzinski, Chapter fourteen - synthesis, characterization, and optical response of gold nanoshells used to trigger release from liposomes, in: N. Düzgünes (Ed.), Methods in Enzymology, Academic Press, 2009, pp. 279–307.
[62] E. Mendoza-Torres, J.A. Riquelme, A. Vielma, A.R. Sagredo, L. Gabrielli, R. Bravo-Sagua, J.E. Jalil, B.A. Rothermel, G. Sanchez, M.P. Ocaranza, S. Lavandero, Protection of the myocardium against ischemia/reperfusion injury by angiotensin-(1–9) through an AT2R and Akt-dependent mechanism, Pharmacol. Res. 135 (2018) 112–121.
[63] B.A. Kindzelski, Y. Zhou, K.A. Horvath, Transmyocardial revascularization devices: technology update, Med. Devices (Auckl) 8 (2014) 11–19.
[64] U.M. Center, Myocardial Revascularization, 2020.